Valence ordering in the intermediate-valence magnet YbPd

Ryo Takahashi,[1] Takashi Honda,[1] Atsushi Miyake,[2] Tomoko Kagayama,[2] Katsuya Shimizu,[2] Takao Ebihara,[3] Tsuyoshi Kimura,[1] and Yusuke Wakabayashi[1,*]

[1]*Division of Materials Physics, Graduate School of Engineering Science, Osaka University, Toyonaka 560-8531, Japan*

[2]*Center for Quantum Science and Technology under Extreme Conditions, Osaka University, Osaka 560-8531, Japan*

[3]*Department of Physics, Faculty of Science, Shizuoka University, Ohya, Shizuoka 422-8529, Japan*

(Received 19 March 2013; revised manuscript received 26 July 2013; published 19 August 2013)

An x-ray diffraction study reveals the valence-ordering structure in an intermediate-valence magnet YbPd with a CsCl structure. The valence of the Yb ions forms an incommensurate structure, characterized by the wave vector (± 0.07 ± 0.07 1/2) below 130 K. At 105 K, the incommensurate structure turns into a commensurate structure, characterized by the wave vector (0 0 1/2). Based on the resonant x-ray diffraction spectra of the superlattice reflections, the valences of the Yb ions below 105 K are found to be 3+ and 2.6+. The origin of the long-wavelength modulation is discussed with the aid of an Ising model having next-nearest-neighbor interaction.

DOI: 10.1103/PhysRevB.88.054109 PACS number(s): 64.70.Rh, 71.28.+d

I. INTRODUCTION

Electronic charges sometimes show intriguing behavior induced by their mutual interactions in condensed matter. Charge ordering is one of the most widely studied phenomena in transition-metal oxides,[1] organic conductors,[2] and rare-earth compounds.[3–5] Normally, charge ordering is seen in materials with low conductivity, and the phenomenon involves a sudden increase in the electrical resistivity. However, YbPd is a good metal in all temperature ranges[6] with resistivity of $\sim 10^2\,\mu\Omega\,\mathrm{cm}$, and is proposed to have a charge order accompanied by a decrease in resistivity.[7,8]

The term "charge order" means slightly different states depending on which one of $2p$, $3d$, or $4f$ electrons is relevant. In charge-ordered organic compounds, occupancy of the molecular orbital is modulated. In $3d$ electron systems, the ionic crystal is a good starting point in many cases. As a result, the carrier density is drastically changed by the charge-ordering transition. In the intermediate-valence Yb compounds, the valence of the Yb ions is the mixture of 2+ (f^{14} configuration, nonmagnetic) and 3+ (f^{13} configuration, magnetic) through the hybridization between conduction bands and $4f$ electrons. The valence state can be changed by electron transfer from the localized f orbital to anions in similarity to the $3d$ cases. Actually, the charge ordering in Yb_4As_3 having formal valences of $Yb^{9/4+}$ and As^{3-} significantly increases the resistivity by reducing the carrier density.[3] By contrast, metallic charge-ordered systems are very different from $2p$ or $3d$ cases. The valence of an ion is defined by the electron occupation number of the f orbital, and the occupation number could vary with the strength of the hybridization between the conduction band and the f bands. Such valence state can form a spatial ordering of the noninteger valence; throughout this paper, we call such structure "valence ordering." Unlike charge-ordering compounds, valence-ordered compounds are metallic as they have electrons in the conduction bands. Since YbPd has no anions and is metallic, the charge-ordering proposed for this compound is called "valence ordering" in this paper.

YbPd is an interesting compound in many ways. In the Yb-Pd phase diagram, this CsCl-structured intermetallic compound stands at the border of Yb^{2+} and Yb^{3+}, which are stabilized on the Yb-rich side and the Pd-rich side, respectively.[9] The valence of the Yb ions in YbPd measured by L_{III}-edge x-ray absorption spectroscopy was actually fractional 2.8+ across all temperature ranges.[6] In the fractional valence state, it shows magnetic ordering at $T_N = 1.9$ K.[7] Magnetic ordering in the fractional valence state is not very common, and we were therefore interested in studying the origin of this rare phenomenon. Mössbauer measurements below 4.2 K show two kinds of Yb, one magnetic and the other nonmagnetic, coexisting in equal proportions.[7] There are five phase transitions, at $T_1 = 125$ K, $T_2 = 105$ K, $T_N = 1.9$ K, $T_{MH} = 0.6$ K, and $T_{ML} = 0.3$ K.[10] While the low-temperature transitions below 2 K are known to be magnetic transitions, the other two transitions have not yet been explained. The high-temperature transitions are accompanied by strong anomalies in the material's specific heat, thermal expansion,[6] and elastic constants.[8] Although these observations collectively suggest that either T_1 or T_2 is the valence-ordering temperature, no superstructure has been reported to date.

In previous reports, broadening of the powder x-ray linewidths makes it difficult to perform structural studies.[7] It was also reported that the valence of the Yb ion at the surface is different from that of the bulk.[11] To overcome these extrinsic problems, we performed bulk-sensitive hard x-ray diffraction measurements on as-grown surfaces of single crystals. Valence ordering can be studied with ordinary x-ray diffraction because of the difference in the ionic radius of Yb^{2+} and Yb^{3+}, which produces a Pd displacement in the valence ordering phase. A more relevant probe for the spatial valence arrangement is resonant x-ray diffraction, which is a combination of an x-ray diffraction technique with spectroscopy. Using the L_{III} absorption edge energy, it is possible to study the valence arrangements of $4f$ electron systems.[4,5] We have succeeded in clearly observing the superstructure induced by valence ordering in YbPd by means of these bulk-sensitive techniques.

II. EXPERIMENT

Single-crystal samples were grown by the self-flux method.[12] The as-grown samples have facets parallel to the {001} planes and are cube shaped. All measurements

were performed on facets to avoid any mechanical stress to the crystal. The typical size of these crystals is 1 mm^3. Nonresonant x-ray diffraction measurements were performed with a four-circle x-ray diffractometer attached to a Mo $K\alpha$ x-ray generator. The incident x-ray beam was monochromatized with a bent graphite monochromator, and the scattered beam was then measured with a charge-coupled device (CCD) camera, a photodiode, or a silicon drift detector. To find the superlattice reflections, x-ray photographs were taken with 18 keV intense synchrotron radiation at the BL-8B beamline of the Photon Factory, KEK, Japan. The valence order was examined with the resonant x-ray diffraction technique at the Yb L_{III} absorption edge. The measurement was performed at the BL-4C beamline of the Photon Factory with a four-circle diffractometer. The sample temperature was controlled using a closed-cycle refrigerator for all measurements.

III. RESULTS AND ANALYSIS

A. Lattice parameters

Figure 1(a) shows the θ-2θ line profiles of $(006)_c$ Bragg reflection at 140 K [above T_1, high-temperature (HT) phase], 115 K [between T_1 and T_2, medium-temperature (MT) phase], and 95 K [below T_2, low-temperature (LT) phase] measured with the Mo $K\alpha$ x-rays. Here, the suffix c denotes the index in the high-temperature cubic phase. In addition to the doublet caused by the $K\alpha_1$ and $K\alpha_2$ x rays, clear peak splitting with an intensity ratio of 1 : 2 was found below T_1. This result indicates that the highly symmetrical YbPd deforms into a tetragonal structure below T_1, and the single crystal turns into a multidomain crystal. Panel (b) shows the lattice parameters a_t and c_t obtained from the peak positions of the $(600)_t$ and $(006)_t$ reflections, where the suffix t denotes the index in the tetragonal phase. Based on the peak profile, we found that T_1 is between 130 K and 135 K. Above T_1, a_t is equal to c_t because the HT phase is cubic. Both of these transitions induce volume expansions with cooling. This behavior agrees well with the slope of the phase boundary in the pressure-temperature phase diagram shown in the inset of panel (b).[10]

The isotropic atomic displacement parameters given by $B = 8\pi\langle u^2\rangle$, where u denotes the atomic displacement from the equilibrium position, for Yb and Pd at 300 K were estimated from the $(00l)_c$ intensities. The parameter values were 0.7 $Å^2$ and 1.4 $Å^2$, respectively. Because the Lindemann melting criterion predicts a value of 0.8 $Å^2$ for B at 300 K, the B for Pd is exceptionally large. The large B value for Pd might thus originate from the fluctuation of the Yb radius caused by the valence fluctuation, although it can be caused by the difference in the atomic mass. Comparison with LuPd helps the interpretation of B parameters.

B. Crystal structure and valence ordering in the LT phase

The synchrotron diffraction experiment was performed to search for superlattice reflections. Figure 2 shows the oscillation photographs around $(136)_c$ taken in (a) the HT phase and (b) the LT phase. Along with the peak splitting caused by the cubic-tetragonal phase transition, the superlattice reflections characterized by the wave vectors $(0\frac{1}{2}0)_c$, $(\frac{1}{2}00)_c$, and $(00\frac{1}{2})_c$ were observed.

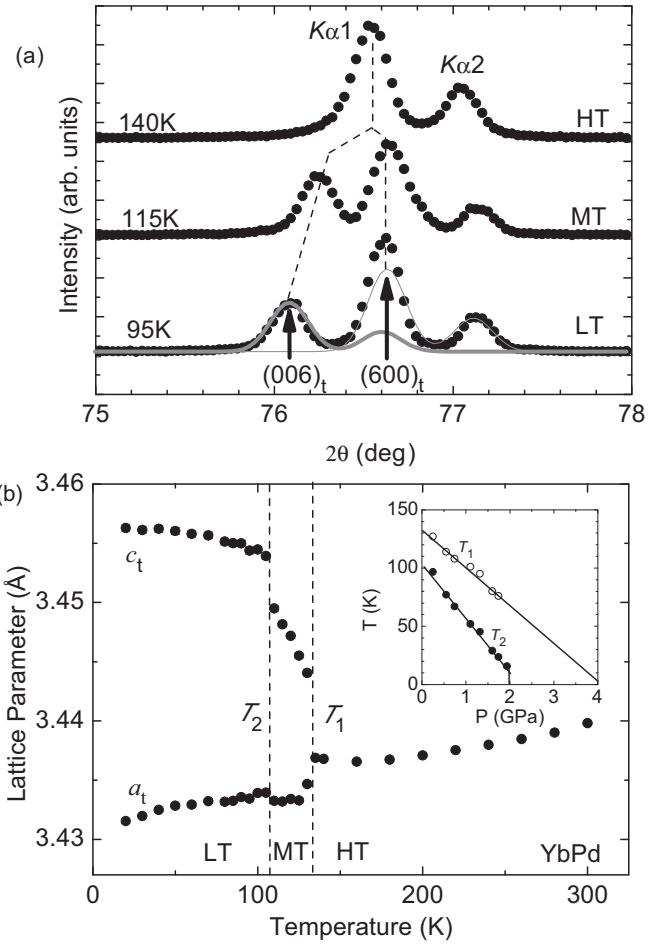

FIG. 1. (a) θ-2θ line profile of $(006)_c$ Bragg reflection at 140 K, 115 K, and 95 K measured with Mo $K\alpha$ x rays. The error bars are shorter than the symbol size. The thick and thin gray curves for the 95 K profile show the results of the peak separation using a double Gaussian for the $K\alpha_{1,2}$ doublet. The dashed lines are intended as visual guides. (b) Temperature variation of the lattice parameters. Inset: Phase diagram reported in Ref. 10.

The positions of the observed superlattice reflections were examined using the four-circle diffractometer. The superlattice reflections in the LT phase were found to be at $(00\frac{1}{2})_t$ away from the fundamental Bragg reflections and no reflections were seen at the $(\frac{1}{2}00)_t$ positions. All the superlattice peaks at either the $(0\frac{1}{2}0)_c$ or $(\frac{1}{2}00)_c$ positions are produced as consequence of the multidomain nature of the cubic-tetragonal phase transition. The peak widths of the superlattice reflections were the same as those of the fundamental Bragg reflections, which means that the correlation of the superstructure reaches a long range. A strong $(0\,0\,6.5)_t$ reflection was observed, whereas $(6\ 0\ \frac{1}{2})_t$ reflection was very weak. This feature indicates that the atomic displacement $\boldsymbol{\delta}$ in the LT phase is parallel to the c axis, because the superlattice reflection intensity caused by the small atomic displacement is proportional to $|\boldsymbol{Q}\cdot\boldsymbol{\delta}|^2$, where $\boldsymbol{Q}$ denotes the scattering vector.[13] We measured the Bragg and superlattice intensities along the $(00l)_t$ line at 95 K to obtain the structure in the LT phase. Figure 2(c) shows the integrated intensities of the $(00l)_t$ peaks plotted against those fitted by the Bs and the $\boldsymbol{\delta}$s along the c axis for both Pd and Yb. It was

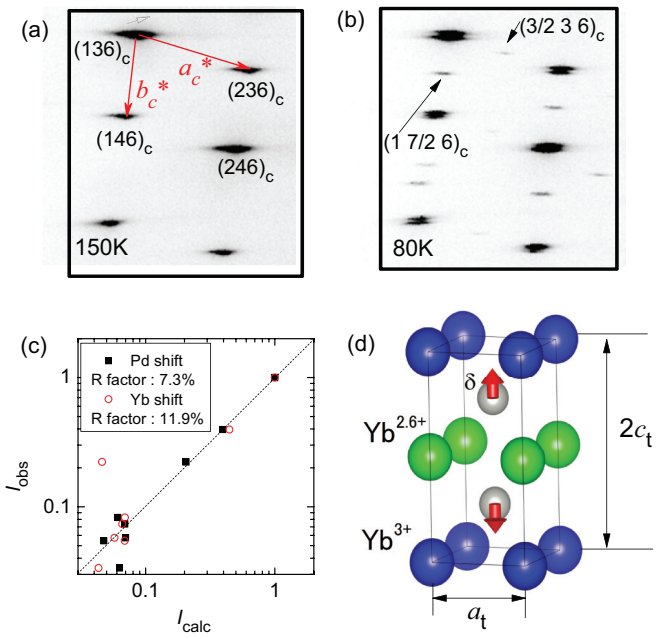

FIG. 2. (Color online) Oscillation photographs around $(136)_c$ taken in (a) the HT phase (150 K) and (b) the LT phase (80 K). (c) Observed intensity at 95 K plotted against the calculated intensity for two structural models: Pd (closed symbol) or Yb (open symbol) displaced from the CsCl structure. (d) Schematic view of the LT phase structure. The magnitude of the displacement δ was found to be 0.11 Å.

found that the Pd atoms are displaced by 0.11 Å along the c direction to form a twofold structure in the LT phase, as shown in Fig. 2(d). If we assume that Pd is not displaced and Yb ions form the twofold structure, the intensity distribution cannot be reproduced as shown in Fig. 2(c) by the open symbols. No atomic displacement was found for the Yb ions; the absence of any Yb displacement was confirmed by the energy spectra of superlattice reflections to be mentioned later. This structure implies an alternate arrangement of high- and low-valence Yb ions along the c direction.

To clarify the valence arrangement, the energy spectra of the superlattice reflections were measured. Each element has a characteristic absorption edge, and the atomic form factor f strongly depends on the x-ray energy E around the edge. Therefore, f is written as $f(Q,E) = f_0(Q) + f'(E) + if''(E)$, where f_0 denotes the Thomson scattering term, and f' and f'' denote the real part and the imaginary part of the anomalous dispersion term, respectively. The characteristic difference in edge energy of divalent and trivalent Yb ions is reported to be 8 eV.[14] This energy difference enables the valence values of these ions to be distinguished. The $f''(E)$ is proportional to $E \cdot \mu(E)$, where $\mu(E)$ denotes the absorption coefficient, and $f'(E)$ is calculated by the Kramers-Krönig transformation. The absorption coefficient $\mu(E)$ shown in Fig. 3(a) was estimated from the experimentally observed Yb $L\alpha$ fluorescence spectrum with a correction[15] for self-absorption effects. The $\mu(E)$ is divided into divalent and trivalent components $\mu_{2+}(E)$ and $\mu_{3+}(E)$ by the relation $\mu(E) = (1 - n_f)\mu_{2+}(E) + n_f\mu_{3+}(E)$, where n_f is the average hole concentration of the Yb f orbital

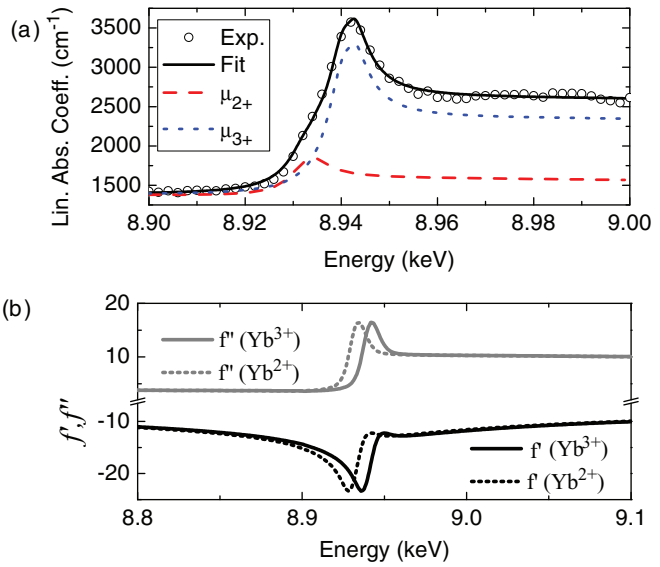

FIG. 3. (Color online) (a) The linear absorption coefficient that was estimated from the fluorescence spectrum. (b) Anomalous scattering factors f' and f'' for Yb^{2+} and Yb^{3+}.

and is set to 0.8 in our analysis.[6] We assumed the relation $\mu_{2+}(E) = \mu_{3+}(E + 8\,\text{eV})$, where $\mu_{3+}(E)$ is described by the sum of a Lorentzian and an arctangent, to reduce the number of parameters. This assumption produces error of $\pm 15\%$ in our estimation of Δ as the estimation of the edge shift might have an error of ± 1 eV. The anomalous scattering factors obtained are shown in Fig. 3(b).

The structure factor F for the superlattice reflections $(00\frac{L}{2})_t$ is written as

$$F_{00\frac{L}{2}} = (-1)^{(L-1)/2} 2 f_{\text{Pd}} \sin(\pi L\delta) + f_H - f_L, \quad (1)$$

$$f_H = (n_f + \Delta) f_{3+} + \{1 - (n_f + \Delta)\} f_{2+}, \quad (2)$$

$$f_L = (n_f - \Delta) f_{3+} + \{1 - (n_f - \Delta)\} f_{2+}, \quad (3)$$

where f_{Pd}, f_{3+}, and f_{2+} denote the atomic form factors for the Pd, Yb^{3+}, and Yb^{2+} ions, δ shows the Pd displacement in the unit of c_t, and Δ denotes the amplitude of the valence ordering. f_H and f_L represent the form factors of high- and low-valent Yb, respectively. The energy dependence of the scattered intensity is $|F|^2/\mu(E)$.[16] The measured energy spectra of the superlattice reflections are shown in Fig. 4 (a), and the absorption corrected spectra are presented in panels (b)–(d). Panels (b)–(d) also show the calculated spectra for three models: (i) Pd displaced by ± 0.11 Å with $\Delta = 0$, (ii) the same lattice distortion with $\Delta = 0.2$, and (iii) Yb displaced by ± 0.05 Å with $\Delta = 0$, which is the structural model producing the $(00l)_t$ intensity shown in Fig. 2(c). The experimentally observed spectra are completely different from the spectra for model (iii), thus confirming that only the Pd atoms are displaced from the CsCl structure in the LT phase. The difference in the valence of Yb ions, Δ, significantly affects the spectral shape of weak reflection, $(00\frac{1}{2})_t$. This is because the relative contribution of the anomalous term, which reflects Δ, in the weak reflection is significant, whereas the Thomson scattering term dominates the scattering amplitude in the stronger reflections. The upturn in the intensity with increasing energy toward the absorption edge seen in panel (b) is not

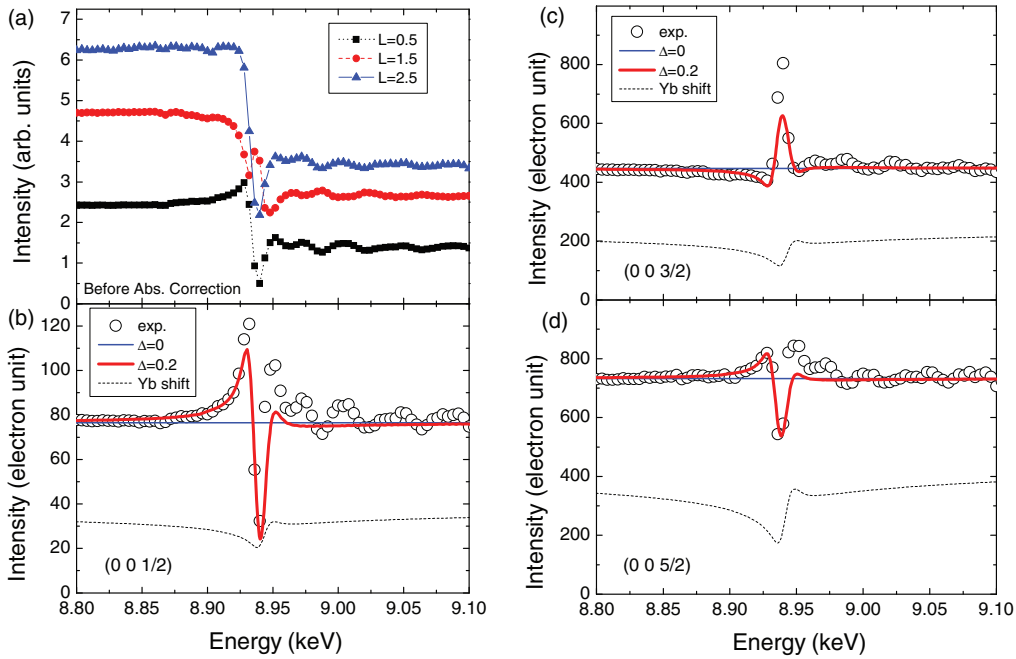

FIG. 4. (Color online) (a) Resonant x-ray diffraction spectra measured at $(00\frac{1}{2})_t$, $(00\frac{3}{2})_t$, and $(00\frac{5}{2})_t$ at 80 K before the absorption correction. Relative intensities of the three reflections are adjusted for presentation. The background intensity was less than the symbol size. (b) Energy spectrum of the $(00\frac{1}{2})_t$ superlattice reflection measured at 80 K. Absorption correction was made (see text). The thick (red) and thin (blue) solid curves show the calculated spectra for $\Delta = 0.2$ and 0, respectively. The dashed curve shows the calculated spectrum based on the structure having Yb displacement. (c) and (d) show those for $(00\frac{3}{2})_t$ and $(00\frac{5}{2})_t$ superlattice reflections, respectively.

expected without valence ordering, as indicated by the thin solid curve, and is therefore a signature of the valence order. Based on a comparison between the experimentally observed spectra and the calculated spectra, we conclude that $\Delta \sim 0.2$, i.e., that the high- and low-valence Yb ions are 3+ and 2.6+, respectively, for the LT phase of YbPd, as shown in Fig. 2(d).

C. Incommensurate structure in the MT phase

In the MT phase, we discovered a splitting of the superlattice reflections. Figure 5(a) shows the scattering intensity distribution of the $(\xi\eta 2.5)_t$ plane at 115 K. There are four peaks at $(\pm x \ \pm x \ 2.5)_t$. Panel (b) shows the line profiles along $(\xi \ \xi \ 2.5)_t$ [the dashed line in panel (a)] at 115 K (MT phase), and at 80 K (LT phase). The peak position, i.e., the incommensurability x, changes from 0.07 in the MT phase to 0 with the phase transition at T_2. This result indicates that the valence order in the MT phase is an alternating arrangement along the c direction, which is similar to that of the LT phase, but it has an in-plane modulation. Similar to the LT phase, the superlattice peaks are as narrow as those of the Bragg reflections, and therefore a long-range correlation was established. The energy spectrum at $(xx0.5)_t$ was similar to Fig. 4(b), showing that this incommensurate structure involves an incommensurate valence arrangement. There are two possible modulation structures, depicted by the stripe-like and checkerboard-like structures that are presented in Fig. 6. The stripe-like structure is characterized by valence modulation along the $[110]_t$ direction with a wavelength of $\sim 7\sqrt{2}a$. This modulation structure provides two superlattice peaks at $(+x \ +x \ 2.5)_t$ and $(-x \ -x \ 2.5)_t$ in the region shown in Fig. 5(a). The other two peaks are produced by the twin variant with a modulation vector along $[1\bar{1}0]_t$. When we adopt the checkerboard-like structure, an alternating arrangement of $7a \times 7a$-sized tiles is expected to produce the four peaks shown in Fig. 5(a).

The temperature variations of the incommensurability and the intensity integrated over all the peaks around $(0\ 0\ 2.5)_t$ are presented in Fig. 5(c). The MT-phase superlattice intensity was found below 140 K, which is slightly above T_1. The inset shows that the peak width of the superlattice intensity above T_1 is broader than the instrumental resolution, meaning that the superstructure is short ranged. The intensity above T_1 is therefore given by the fluctuation. The intensity is proportional to the square of the Pd displacement, which must be a good indicator of the Yb valence. Below $T_2 = 105$ K, the intensity is nearly constant, which means that the valence-order amplitude in the LT phase is independent of temperature. The incommensurability varies gradually in the MT phase, and drops to zero at T_2. The absence of the higher harmonic peaks at $(\pm nx \ \pm nx \ 2.5)_t$ (where n is an integer) and the sudden decrease in the total intensity at T_2 with heating indicate that the modulation is sinusoidal.

IV. DISCUSSION

There are two possible interpretations of the intensity distribution in the MT phase: stripe-like and checkerboard-like structures as shown in Fig. 6. While we have no decisive data to distinguish the two structures, the stripe-like model is the more plausible of the two. In Fig. 5(a), there are some

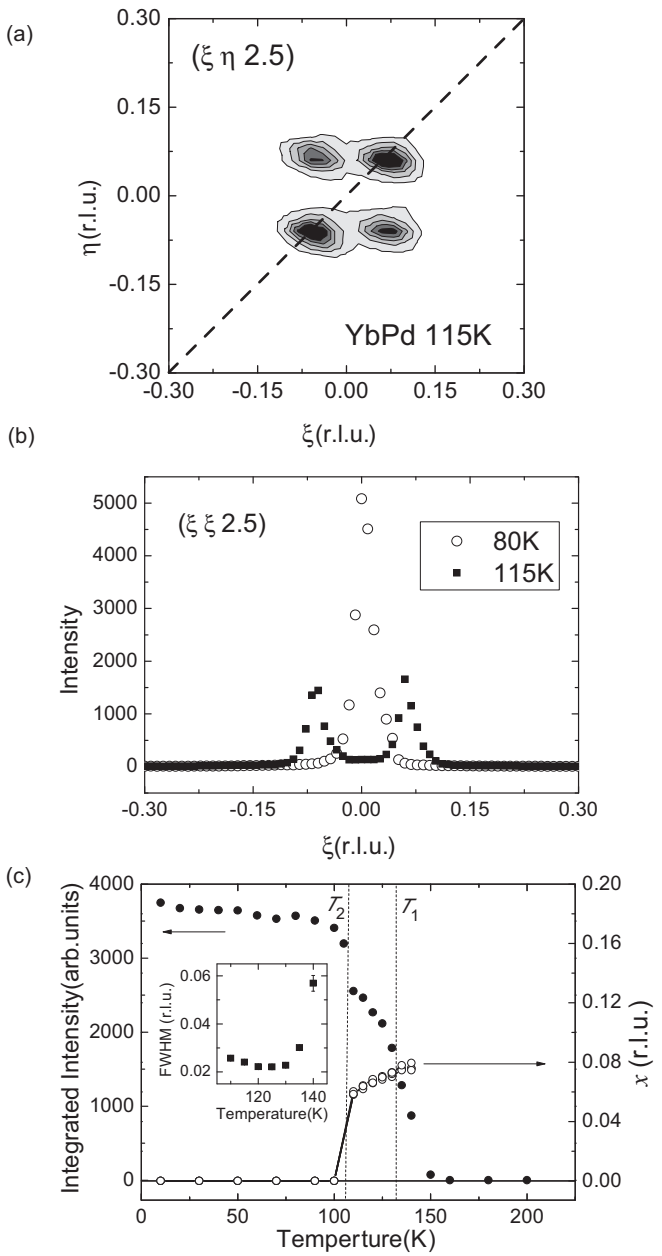

FIG. 5. (a) Scattering intensity distribution of the $(\xi\eta 2.5)_t$ plane at 115 K. (b) Line profiles along the dashed line in panel (a) at 115 K and 80 K. (c) Temperature dependence of the incommensurability x and the integrated intensity. Inset: Temperature variation of the incommensurate peak along the $[110]_t$ direction.

differences in the intensities of the four peaks. The intensity at $(+x,+x,2.5)_t$ is equal to that at $(-x,-x,2.5)_t$, and the intensity at $(+x,-x,2.5)_t$ is equal to that at $(-x,+x,2.5)_t$. However, the former pair is apparently stronger than the latter pair. This difference is accounted for by the domain ratio in the stripe-like model, while the checkerboard-like model cannot account for this intensity difference.

Next, we examine the origins of the incommensurate structure based on the stripe-like model. The valence states of the ions can be treated as Ising pseudospins.[17] It has long been known that an Ising spin with a ferro-coupling for the nearest neighbor ($J_1 > 0$) and an antiferro-coupling for the second neighbor ($J_2 < 0$), i.e., the axial next-nearest-neighbor Ising (ANNNI) model, results in an intricate phase diagram that involves wide incommensurate regions and commensurate regions separated by the first-order phase transitions.[18,19] The ANNNI model has been applied to $4f$ electron magnets including CeSb,[20] CeBi,[21] and UPd_2Si_2,[22] to ferroelectrics such as $NaNO_2$[23] and $[N(CH_3)_4]_2MCl_4$,[24] and to charge/valence ordering systems such as NaV_2O_5[25] and EuPtP.[5] Among these materials, EuPtP has significant similarities to YbPd, because both are metallic valence-fluctuating compounds.

Let us compare the known properties of the valence ordering in YbPd with those expected from the ANNNI model. First, the characteristic modulation vector varies from (0.07, 0.07, 0) at T_1 to (0.06, 0.06, 0) at T_2. According to Ref. 18, the wavelength is stabilized in a narrow temperature range with $-J_2/J_1 \sim 0.27$. When the temperature decreases, the calculation then predicts a first-order phase transition to a ferroic arrangement within the c plane, which was observed in our experiments at T_2. The ratio $-J_2/J_1$ is controlled by the application of pressure.[24,25] As shown in the inset of Fig. 1(b), the LT phase vanishes around 2 GPa, whereas the MT phase remains above that pressure level. When we simply map the ANNNI phase diagram to the YbPd temperature-pressure phase diagram, then the valence order characterized by the wave vector $(\frac{1}{4}\frac{1}{4}\frac{1}{2})$, which corresponds to $2\sqrt{2}a$ in-plane periodicity, is expected for the ground state under pressures of more than 2 GPa. It is also expected that a large number of phase transitions will occur in the MT phase. We can test the applicability of the ANNNI model to YbPd by performing further diffraction measurements in high-pressure environments.

Another common origin of the long-wavelength modulation is Fermi surface nesting. However, the nesting vector can vary only moderately. The cell volume change at T_2 is almost the same as that within the MT phase, which means that the change

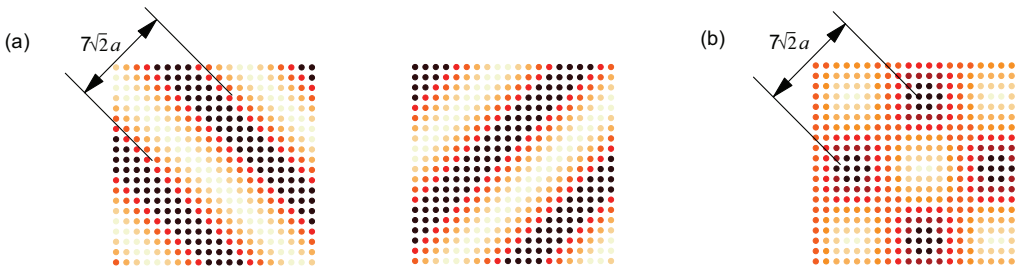

FIG. 6. (Color online) Schematics of the possible modulation structures in the MT phase. (a) Stripe structure; (b) checkerboard-like structure. The difference in color represents the Yb valence.

in the Fermi wave vector at T_2 should be at a similar level to the change within the MT phase. As shown in the temperature dependence of the incommensurability x [Fig. 5(c)], the drop in x at T_2 is far greater than its shift in the MT phase. Therefore, the long-wavelength modulation is unlikely to be caused by nesting of the Fermi surface.

Finally, we discuss the effects of the valence ordering on the magnetic and conductive properties of the material. The application of pressure makes the LT phase unstable, and the ground-state valence-ordering structure is changed from an $x = 0$ structure to an $x \neq 0$ structure (the MT structure) above 2 GPa. In accordance with this transition, T_N vanishes.[26] Therefore, the magnetic ordering at T_N requires a valence-ordered structure in the LT phase. The valence ordering characterized by $x = 0$ makes Yb^{3+} and $Yb^{2.6+}$ sublattices, which can have different Kondo temperatures. The Yb^{3+} sublattice can form a magnetic order because it is not in the mixed valence state. In the $x \neq 0$ structure in which the sinusoidal valence modulation develops, the Yb^{3+} content is small, and therefore the magnetic ordering is suppressed.

Electric resistivity of charge-ordering Yb_4As_3 shows sudden increase at the charge-ordering temperature because of the decrease of the carrier density. In EuPtP, which shows two valence-ordering transitions at 247 K and 201 K,[5] resistivity increases and decreases at each transition temperature with cooling.[27] In EuPtP, the average valence of Yb is also changed at the valence-ordering transition temperatures and therefore the resistivity is affected by both valence transition and valence ordering. In YbPd, the average valence is unchanged; thus one can find the effect of the valence ordering clearly. Temperature variation of the resistivity of YbPd is reported in Ref. 6. They reported sudden decreases in resistivity with cooling at both T_1 and T_2. This change in resistivity is induced by the decrease in the randomness of the valence arrangement, since the randomness causes a scattering of conduction electrons. In the LT phase, YbPd still has much larger resistivity than LuPd.[6] This is qualitatively understood by the electron scattering of the $Yb^{2.6+}$ site.

V. SUMMARY

We have performed a series of x-ray diffraction measurements on the valence-fluctuating compound YbPd. The material shows twofold charge ordering characterized by the wave vector $(00\frac{1}{2})_t$ below 105 K. Between 105 K and 130 K, the charge-ordering structure is modulated, and the characteristic wave vector is $(\pm x, \pm x, \frac{1}{2})_t$ with $x \sim 0.07$. We propose that this long-wavelength structure is described using the ANNNI model; this interpretation can be examined by diffraction measurements under high pressures.

Note added in proof. The $(00\frac{1}{2})_c$ superlattice reflections in the LT phase are also reported by another group very recently,[28] while they provide no quantitative analysis of the atomic displacement.

ACKNOWLEDGMENTS

This work was supported by KAKENHI (Grant No. 23684026), the Japan Securities Scholarship Foundation, and the Global COE Program (G10).

*wakabayashi@mp.es.osaka-u.ac.jp

[1] M. Imada, A. Fujimori, and Y. Tokura, Rev. Mod. Phys. **70**, 1039 (1998).
[2] H. Seo, C. Hotta, and H. Fukuyama, Chem. Rev. **104**, 5005 (2004).
[3] A. Ochiai, T. Suzuki, and T. Kasuya, J. Phys. Soc. Jpn. **59**, 4129 (1990).
[4] U. Staub, M. Shi, C. Schulze-Briese, B. D. Patterson, F. Fauth, E. Dooryhee, L. Soderholm, J. O. Cross, D. Mannix, and A. Ochiai, Phys. Rev. B **71**, 075115 (2005).
[5] T. Inami, S. Michimura, A. Mitsuda, and H. Wada, Phys. Rev. B **82**, 195133 (2010).
[6] R. Pott, W. Boksch, G. Leson, B. Politt, H. Schmidt, A. Freimuth, K. Keulerz, J. Langen, G. Neumann, F. Oster, J. Röhler, U. Walter, P. Weidner, and D. Wohlleben, Phys. Rev. Lett. **54**, 481 (1985).
[7] P. Bonville, J. Hammann, J. A. Hodges, P. Imbert, and G. J. Jéhanno, Phys. Rev. Lett. **57**, 2733 (1986).
[8] Y. Nakanishi, T. Kamiyama, K. Ito, M. Nakamura, M. Sugishima, A. Mitsuda, H. Wada, and M. Yoshizawa, Chinese J. Phys. **49**, 462 (2011).
[9] A. Iandelli and A. Palenzona, Rev. Chim. Miner. **10**, 303 (1973).
[10] A. Miyake, T. Kagayama, K. Shimizu, and T. Ebihara, J. Phys.: Conf. Ser. **391**, 012045 (2012).
[11] M. Domke, C. Laubschat, E. V. Sampathkumaran, M. Prietsch, T. Mandel, G. Kaindl, and H. U. Middelmann, Phys. Rev. B **32**, 8002 (1985).
[12] P. C. Canfield and Z. Fisk, Philos. Mag. B **65**, 1117 (1992).
[13] The scattering amplitude from a crystal with a structural modulation is $F(\boldsymbol{Q}) = \sum_n f_n \exp[i\boldsymbol{Q} \cdot (\boldsymbol{R}_n + \boldsymbol{\delta}_n)] \simeq \sum_n f_n \exp[(i\boldsymbol{Q} \cdot \boldsymbol{R}_n)(1 + i\boldsymbol{Q} \cdot \boldsymbol{\delta}_n)]$, where $\boldsymbol{R}_n$ and $\boldsymbol{\delta}_n$ denote the average atomic position and atomic displacement of the nth atom. The amplitude proportional to $\boldsymbol{Q} \cdot \boldsymbol{\delta}_n$ corresponds to the superlattice reflection, whereas the rest of the amplitude corresponds to the Bragg reflection. The superlattice intensity is thus proportional to $|\boldsymbol{Q} \cdot \boldsymbol{\delta}|^2$.
[14] J. Röhler, in *Handbook on the Physics and Chemistry of Rare Earths*, edited by K. A. Gschneidner, Jr., L. Eyring, and S. Hüfner, Vol. 10 (North-Holland, Amsterdam, 1987), p. 453.
[15] S. W. Lovesey and S. P. Collins, *X-Ray Scattering and Absorption by Magnetic Materials* (Oxford University Press, New York, 1996).
[16] K. Dumesnil, A. Stunault, Ph. Mangin, C. Vettier, D. Wermeille, N. Bernhoeft, S. Langridge, C. Dufour, and G. Marchal, Phys. Rev. B **58**, 3172 (1998).
[17] While the MT phase has a sinusoidal modulation, the Ising model can be relevant because the thermal average of the Ising pseudospins can show intermediate values.
[18] P. Bak and J. von Boehm, Phys. Rev. B **21**, 5297 (1980).
[19] M. E. Fisher and W. Selke, Phys. Rev. Lett. **44**, 1502 (1980).
[20] J. von Boehm and P. Bak, Phys. Rev. Lett. **42**, 122 (1979).
[21] G. Uimin, J. Phys. Lett. **43**, 665 (1982).
[22] T. Honma, H. Amitsuka, S. Yasunami, K. Tenya, T. Sakakibara, H. Mitamura, T. Goto, G. Kido, S. Kawarazaki, Y. Miyako, K. Sugiyama, and M. Date, J. Phys. Soc. Jpn. **67**, 1017 (1998).

[23]W. Selke and P. M. Duxbury, Z. Phys. B **57**, 49 (1984).
[24]S. Shimomura, N. Hamaya, and Y. Fujii, Phys. Rev. B **53**, 8975 (1996).
[25]K. Ohwada, Y. Fujii, N. Takesue, M. Isobe, Y. Ueda, H. Nakao, Y. Wakabayashi, Y. Murakami, K. Ito, Y. Amemiya, H. Fujihisa, K. Aoki, T. Shobu, Y. Noda, and N. Ikeda, Phys. Rev. Lett. **87**, 086402 (2001).
[26]A. Miyake, K. Kasano, T. Kagayama, K. Shimizu, R. Takahashi, Y. Wakabayashi, T. Kimura, and T. Ebihara, J. Phys. Soc. Jpn. **82**, 084706 (2013).
[27]A. Nowack, J. Klug, N. Lossau, and A. Mewis, Z. Phys. B **77**, 381 (1989).
[28]A. Mitsuda, M. Sugishima, T. Hasegawa, S. Tsutsui, M. Isobe, Y. Ueda, M. Udagawa, and H. Wada, J. Phys. Soc. Jpn. **82**, 084712 (2013).